Main Manuscript for

PLCβs are recruited to the plasma membrane in macrophages by both Gβγ and $G\alpha_q$

Maria E. Falzone[1,2,3], Priyam Banerjee[4], Roderick MacKinnon[1,2]

[1]Laboratory of Molecular Neurobiology and Biophysics, The Rockefeller University, NY, United States. [2]Howard Hughes Medical Institute, The Rockefeller University, NY, United States. [3]Present Address: Department of Biochemistry and Structural Biology and Greehey Children's Cancer Research Institute, University of Texas Health Science Center at San Antonio, TX, United States. [4]Bio-Imaging Resource Center, The Rockefeller University, NY, United States.

*Roderick MacKinnon

Email: mackinn@rockefeller.edu

Author Contributions: R.M. and M.E.F. designed studies; M.E.F. and P.B. performed experiments; R.M. M.E.F. and P.B. analyzed and interpreted data; R.M. M.E.F. and P.B, wrote the paper.

Competing Interest Statement: The authors declare no competing interests.

Classification: Biological Sciences, Biochemistry.

Keywords: PLCβ3, PIP2, Gβγ, GPCR signaling, Macrophages

This PDF file includes:

Main Text
Figures 1 to 6
Table 1

Abstract

PLCβ enzymes cleave PIP2 from the plasma membrane, producing IP3 and DAG, which regulate intracellular Ca^{2+} levels and protein kinase C activity, respectively. They are regulated by GPCR signaling through the G proteins Gβγ and $G\alpha_q$ and have been shown to function as coincidence detectors for dual stimulation of $G\alpha_q$ and $G\alpha_i$-coupled receptors via these G proteins. PLCβs are aqueous-soluble enzymes, but partition onto the membrane surface to access their lipid substrate. We previously demonstrated that membrane recruitment and orientation of the catalytic core on the membrane surface underlie Gβγ-dependent regulation of PLCβ enzymes. Using macrophages as a model system, where PLCβ signaling is essential for responses to infection and tissue injury, we investigated the contribution of Gβγ-dependent regulation and membrane recruitment of PLCβ in the context of endogenous signaling. By measuring Ca^{2+} mobilization, we demonstrate that both $G\alpha_i$ and $G\alpha_q$-coupled receptors independently stimulate PLCβ activity, illustrating that Gβγ alone is sufficient to activate PLCβ in certain contexts. Using total internal reflection and stimulated emission depletion microscopy, we demonstrate that most of the PLCβ3 in the cell is localized away from the plasma membrane at rest but is rapidly recruited to the plasma membrane upon stimulation by both $G\alpha_i$ and $G\alpha_q$-coupled receptors, illustrating that both Gβγ and $G\alpha_q$ recruit PLCβ to the plasma membrane. These results support an updated model for G protein-dependent regulation of PLCβ enzymes, where Gβγ-induced regulation in the absence of $G\alpha_q$ is context dependent and dictated by the local concentration of receptor, G proteins, and PLCβ.

Significance Statement

PLCβ enzymes are critical mediators of signal transduction with roles in neuronal, cardiac, and immunological signaling. Despite this importance, many aspects of their function and regulation remain poorly understood. PLCβs are aqueous soluble but must partition onto the membrane surface to access their lipid substrate, which enables regulation at the partitioning step, the catalytic step, or both. We previously demonstrated that membrane recruitment and orientation of the catalytic core on the membrane surface underlie the PLCβ regulation by one effector, Gβγ. Using macrophages as a model system for physiological signaling, we demonstrate that Gβγ is capable of independently activating PLCβ via membrane recruitment under the conditions of endogenous signaling.

Main Text

Introduction

PLCβ enzymes are canonical downstream effectors of G protein coupled receptor (GPCR) signaling (3-5). Upon activation, PLCβ enzymes cleave PIP2 from the plasma membrane, producing inositol triphosphate (IP3) and DAG (6, 7). IP3 opens the IP3 receptor ion channel on the endoplasmic reticulum (ER), leading to an increase in cytosolic Ca^{2+} concentration and DAG activates protein kinase C (PKC). PLCβ function is essential for a multitude of cellular processes, including cardiac signaling, neuronal signaling, and macrophage activation (3-5). Accordingly, their activity needs to be tightly regulated, with very low basal activity and robust stimulus-dependent activation. PLCβs are under the control of both $G\alpha_q$ and $G\alpha_i$-dependent GPCR signaling through direct interactions with the G proteins $G\alpha_q$ and Gβγ (3, 5). They have also been shown to function as coincidence detectors for co-stimulation of $G\alpha_q$ and $G\alpha_i$-coupled receptors through simultaneous activation by both G proteins (3-5).

Using *in vitro* reconstitution experiments, we previously demonstrated that Gβγ and $G\alpha_q$ activate PLCβ via differing mechanisms, Gβγ by recruiting PLCβ to the membrane and orienting the catalytic

core for substrate binding and catalysis and $G\alpha_q$ by increasing the catalytic rate constant, k_{cat}, by displacing an autoinhibitory loop from the active site (1, 2). Additionally, we showed that dual stimulation by both G proteins is mediated by the combined effects of these differing activation mechanisms. Thus, together, both G proteins activate to the order of the product of each individual effect (1). These observations led us to propose that a combination of autoinhibition and robust stimulus-dependent activation allow PLCβ enzymes to be tightly regulated by GPCR signaling and prevent aberrant signaling.

While we and others have demonstrated that Gβγ robustly activates PLCβ enzymes in reconstituted systems (2, 8-11), the role and feasibility of independent regulation of PLCβ enzymes by Gβγ in the cellular context has come under debate. Pertussis toxin (PTX)-sensitive and Gβγ-dependent regulation of PLCβs has been reported for decades (3, 5), leading to the proposal that Gβγ released from $G\alpha_i$-coupled receptor signaling could activate PLCβs independently of $G\alpha_q$ (12, 13). However, several recent reports have proposed that the presence of $G\alpha_q$ is strictly required for any Gβγ-dependent activation (14-18). Macrophages are one cellular system that have been shown to support both $G\alpha_i$ and $G\alpha_q$-dependent PLCβ activity, where both pathways play important roles in macrophage activation in response to cellular injury and infection (12, 19-21). To understand how G protein regulation of PLCβs is manifested in the native cellular context, and whether each pathway can separately influence PLCβ activity, we studied this cellular system.

Using Raw264.7 cells, a mouse macrophage cell line with endogenous $G\alpha_i$ and $G\alpha_q$-dependent PLCβ activation and coincidence detection, we investigated the regulation of PLCβ activity and the role of membrane recruitment in this regulation. Importantly, we used the endogenous signaling components without overexpression to study signaling in the native context. Our results show that $G\alpha_i$-coupled signaling is sufficient to activate PLCβ robustly in the absence of $G\alpha_q$ stimulation and appears to do so by recruiting PLCβ to the plasma membrane on a functionally relevant timescale. These observations lead us to propose that the ability of $G\alpha_i$ signaling to activate PLCβ enzymes is context-dependent and likely dictated by the concentration and distribution of receptor, G proteins, and PLCβ.

Results

Stimulation of Raw264.7 cells with GPCR agonists results in PLCβ-dependent Ca^{2+} transients

To confirm the presence of GPCR-dependent PLCβ activity in Raw264.7 cells, we measured PLCβ-dependent increases in cytoplasmic Ca^{2+} concentration using a fluorescent Ca^{2+} indicator. Wildtype Raw264.7 cells were loaded with Fluo-4 AM (**Fig. 1A**), followed by subsequent stimulation with agonists for three different receptors: a complement receptor (C5aR), a purinergic receptor (P2Y6R), and a lysophosphatidic acid receptor (LPAR). The agonist C5a activates C5aR, which is part of the complement pathway and plays a role in macrophage activation and response to infection (22). The agonist UDP signals through P2Y6R and plays a role in macrophage activation in response to tissue injury (23). The agonist LPA signals via LPAR and plays a role in macrophage activation and inflammation (24). In agreement with previous results, addition of saturating concentrations of all three agonists lead to rapid Ca^{2+} transients, which peak ~10s following stimulation and decay to baseline over 40-100s (**Fig. 1B, S1A**) (12, 19, 25). Treatment with PLCβ inhibitor U73122 blocked these Ca^{2+}-transients, whereas vehicle (DMSO) and U73342, the established negative control compound without PLCβ inhibitory activity, had only small reductions in peak height and slope, indicating these transients are PLCβ-dependent (**Fig. 1C, S1**).

G protein coupling of P2Y6R, C5aR, and LPAR

Many GPCRs couple to multiple G proteins. In order to assess the role of $G\alpha_i$ versus $G\alpha_q$-coupling in regulation of PLCβ enzymes, we sought to define the G protein coupling of our three receptors

using FR900359 (FR) and YM254890 (YM), cyclic peptide inhibitors that selectively block $G\alpha_q$ trimer release (26), and pertussis toxin (PTX), which selectively blocks $G\alpha_i$ trimer release (27) (**Fig. 1D, G**). Blocking $G\alpha_q$ trimer release completely inhibited UDP and LPA-dependent Ca^{2+} increases, whereas blocking $G\alpha_i$ signaling inhibited most of the C5a-dependent Ca^{2+} increase with minimal effect on the UDP-dependent increase (**Fig. 1D-I, S2A-C**). These observations indicate that UDP and LPA signal through $G\alpha_q$ and C5a signals through $G\alpha_i$ in macrophages, consistent with previous results (12, 19, 20). Small decreases in UDP and LPA-induced Ca^{2+} peak height and slope in the presence of PTX (**Fig. 1H-I, S2A-C**) are likely due to non-specific toxicity, since their effects are completely blocked by FR/YM treatment, indicating they are completely dependent on $G\alpha_q$. Importantly, C5a-dependent Ca^{2+} transients are intact upon FM and YR treatment, demonstrating that $G\alpha_q$ is not required for $G\alpha_i$-dependent PLCβ activation in macrophages, consistent with previous results (12).

Dual stimulation of C5aR and P2Y6

We next sought to evaluate the effect of dual stimulation of $G\alpha_i$- and $G\alpha_q$-coupled receptors on PLCβ activation. We combined maximal concentrations of C5a and UDP and measured the corresponding Ca^{2+} increases. While the peak fluorescence did not increase on the order of the sum of each agonist alone, the transients arose significantly faster than in the presence of each ligand on its own (**Fig. 2A-B**). To quantify the rate of transient increase, we fit the early rise of the Ca^{2+} signal to a straight line and compared the slopes (**Fig. 2B-C**). The slope upon dual stimulation is significantly greater than the sum of the slopes of the individual stimuli (**Fig. 2C**), suggesting that the largest effect of dual stimulation is a faster Ca^{2+} increase. The activation of PLCβ in response to dual stimulation of $G\alpha_i$ and $G\alpha_q$-coupled receptors approaches the product of each ligand on its own, which is consistent with previous work and our *in vitro* results (1, 12). Additionally, upon inhibition of $G\alpha_i$ or $G\alpha_q$-dependent signaling using PTX or FM/YR, the slopes of the Ca^{2+} increases return to the level of each agonist on its own, pointing to the absence of additional synergy in this regulation (**Fig. S2D-F**).

Both $G\alpha_q$ and $G\alpha_i$-dependent signaling recruit PLCβ3 to the plasma membrane

We next studied the PLCβ cellular distribution and how it is influenced by GPCR stimulation using immunolabeling with primary and secondary antibodies. We used a primary antibody specific for mouse PLCβ3, which has been shown to underlie coincidence detection in Raw264.7 cells (12), and mouse C5aR to serve as a plasma membrane marker. We investigated the cellular distribution of PLCβ3 and its recruitment to the plasma membrane using three different types of microscopy to enable a comprehensive assessment (**Fig. S3A**).

To get a broad overview of the PLCβ3 present on the plasma membrane and how it is influenced by agonist stimulation, we used Total Internal Reflection (TIRF) microscopy, with a penetration depth of ~100 nm (28) (**Fig. S3A, C**). In the absence of stimulation, we observed PLCβ3 puncta with a mean density of ~0.2/μm^2 and a spot area of ~0.13 μm^2. This spot area is ~2-fold larger than expected for the diffraction limited spot diameter of 0.250 μm (~0.05 μm^2), which could be due to clusters of several PLCβ3 proteins. Upon stimulation for 3-120s with UDP, C5a, or both, we observed a significant increase in PLCβ3 spot density and size (**Fig. 3**), suggesting PLCβ3 is recruited to the plasma membrane upon receptor activation. Stimulation with C5a significantly increased PLCβ3 spot density after 5s and spot size after 10s, with a maximal increase of ~3-fold for both size and density after 120s (**Fig. 3F, I**). Stimulation with UDP significantly increased PLCβ3 spot density after 10s and spot size after 5s, with a maximal increase of 2-fold for both spot size and density after 60s (**Fig. 3G, J**). Stimulation with both agonists significantly increased PLCβ3 spot size and density at 5s, with a maximal effect of ~4-fold for density and ~3-fold for size after 120s (**Fig. 3H, K**), consistent with our functional experiments in that the biggest effect of dual

141 stimulation is a faster response. Otherwise, there is no significant difference between dual
142 stimulation and C5a stimulation alone.

143 In our functional experiments, the Ca^{2+} transient peaks ~10s after stimulation and then decays over
144 40-100s. In contrast, PLCβ3 puncta at the plasma membrane continue increasing in size and
145 density as stimulation time increases up to 120s. This discrepancy is likely due to tight cellular
146 control of cytoplasmic Ca^{2+} concentration, the readout used in our functional assay, as it is likely
147 pumped back into the ER despite continued stimulation. Alternatively, the short timescale of our
148 functional signal could be due to depletion of PIP2 from the plasma membrane. Accordingly, we
149 focus on PLCβ3 function within 10s of stimulation (**Fig. S3B**), what we consider to be a functionally
150 relevant timescale. Our data suggest that both UDP and C5a recruit PLCβ3 to the plasma
151 membrane on this timescale.

152 *PLCβ is mostly localized in the interior of the cell at rest*

153 To gain information about PLCβ3 distribution across the cell volume, we carried out 3D Stimulated
154 Emission Depletion (STED) microscopy axial line scans on Raw264.7 cells fixed and stained for
155 PLCβ3 and C5aR (**Fig. 4, S3A**) (29). A major advantage of the 3D STED technique is its ability to
156 resolve structures at isotropic (X,Y,Z) super-resolution beyond the diffraction limit, down to ~80-
157 100nm (**Fig. S3A**) (29). We used the C5aR signal to trace the plasma membrane and quantified
158 the percent of PLCβ3 puncta within 100 nm, corresponding to the resolution limit. In the absence
159 of stimulation, PLCβ3 is predominately localized in the interior of the cell, with only ~20% of puncta
160 at the plasma membrane (**Fig. 4**). Upon stimulation with UDP, C5a, or both, the percentage of
161 PLCβ3 puncta at the plasma membrane increases, consistent with the results observed with TIRF
162 microscopy. However, only C5a and the combination of both agonists have a significant effect over
163 the functionally relevant timescale of 10s (**Fig. 4**). Stimulation with UDP increases the percentage
164 of PLCβ3 puncta at the plasma membrane ~1.3-fold after 60s of stimulation (**Fig. 4G**). Stimulation
165 with C5a and both agonists increase the percentage of puncta of PLCβ3 at the plasma membrane
166 ~1.7-fold after 60s of stimulation (**Fig. 4F, H**). While the outcome of 3D STED shows a statistically
167 significant trend over a limited range, we investigate membrane partitioning of PLCβ next using a
168 different approach.

169 *$G\alpha_i$-coupled signaling is more efficient at recruiting PLCβ3 to the plasma membrane at short time*
170 *scales*

171 To obtain information about the PLCβ3 distribution on the plasma membrane in a different way, we
172 used super-resolution 2D STED imaging, which permits higher 2D (X,Y) resolution (~40-50 nm)
173 (**Fig. S3**) (29). We collected z-stacks of the plasma membrane of Raw264.7 cells fixed and stained
174 for PLCβ3 and C5aR, guided by the C5aR signal as a plasma membrane marker. In the absence
175 of stimulation, the PLCβ3 density was ~4 puncta/μm^3 with an average puncta lateral diameter of
176 0.07 μm, suggesting that the spots observed in the TIRF imaging are sometimes due to multiple
177 PLCβ3s within the 0.250 μm diffraction-limited resolution. We observe clear recruitment of PLCβ3
178 to the plasma membrane upon stimulation with $G\alpha_i$ or $G\alpha_q$-coupled agonists. Upon stimulation with
179 C5a, the PLCβ3 puncta density is increased by ~2.5-fold after 10s, (**Fig. 5C-E**). Upon stimulation
180 with UDP, the PLCβ3 puncta density is increased by ~2.5-fold after 60s but not after 10s, consistent
181 with the 3D STED measurements (**Fig. 5F-H**) Finally, upon stimulation with both agonists, the
182 PLCβ3 puncta density is increased ~2.5-fold at 10s and ~3-fold at 60s (**Fig. 5I-K**). Across all
183 stimulation conditions, the PLCβ3 X-Y diameter did not change significantly.

184 Quantification of object number and geometry in light microscopy approaches is dependent on the
185 signal threshold used for segmentation. To reduce bias, we completed the analysis of our 2D STED
186 data at a low segmentation threshold **(Fig. S4)**. With low thresholds, the density of PLCβ3 on the
187 plasma membrane was ~1.7 puncta/μm^3 with an X-Y diameter of ~0.08 μm. The increases in

188 PLCβ3 density at the plasma membrane upon stimulation with C5a, UDP, or both were consistent
189 with the higher segmentation thresholds, suggesting our measurements scaled proportionately with
190 signal thresholds, and that our conclusions are robust to variations in signal threshold over the
191 tested range.

192 *C5aR density at the plasma membrane increases upon C5a stimulation*

193 C5aR was used as a plasma membrane marker in our 2D STED experiments, which enabled
194 analysis of its puncta density and size. At rest, the C5aR density was ~10 puncta/μm^3 with an X-Y
195 diameter of ~0.12 μm, consisting of larger and more concentrated puncta than PLCβ (**Fig. S5**).
196 Upon stimulation with C5a, we observed the density and diameter of C5aR puncta increased ~1.5-
197 fold (**Fig. S5**). This effect was not observed upon stimulation with an unrelated agonist, UDP. In
198 the presence of both agonists, the increases are evident but smaller. These observations suggest
199 that receptor mobilization may play a role in cellular responses to C5a stimulation.

200 **Discussion**

201 This study aims to elucidate the role and mechanism of Gβγ-dependent activation of PLCβ enzymes
202 in the cellular context. We previously demonstrated that Gβγ robustly activates PLCβ via membrane
203 recruitment and orientation using *in vitro* reconstitution studies (1, 2). However, the question of
204 whether Gβγ recruits PLCβ to the membrane and its ability to independently regulate PLCβ in the
205 cellular environment is debated. To address this question, we used a mouse macrophage cell line,
206 Raw264.7 cells, to study GPCR-dependent regulation of PLCβ function and cellular localization.
207 Using endogenous proteins to observe native signaling, our experiments show that stimulation of
208 both $G\alpha_q$ and $G\alpha_i$-coupled receptors induce PLCβ-dependent Ca^{2+} transients (**Fig. 1-2**). $G\alpha_i$-
209 dependent signaling was intact upon treatment with FR/YM, cyclic peptide inhibitors that block $G\alpha_q$
210 trimer dissociation, demonstrating that $G\alpha_q$ is dispensable for $G\alpha_i$-dependent PLCβ activation in
211 this context (**Fig. 1**). Using immunolabeling coupled with three complementary fluorescence
212 microscopy modalities (**Fig. S3A**), this work demonstrates that most of the PLCβ3 in macrophages
213 (~80%) is localized in the interior of the cell, away from the plasma membrane, which is consistent
214 with previous results (18). Upon GPCR stimulation, PLCβ3 is recruited to the plasma membrane.
215 Signaling from both $G\alpha_q$ and $G\alpha_i$-coupled receptors induced recruitment of PLCβ3 to the plasma
216 membrane, indicating that both G proteins, Gβγ and $G\alpha_q$, induce PLCβ3 membrane recruitment.
217 Recruitment of PLCβ3 by $G\alpha_q$-dependent signaling was recently demonstrated (18), but this is the
218 first demonstration of membrane recruitment by $G\alpha_i$-dependent signaling.

219 Analysis of our TIRF images reveals an increase in PLCβ3 spot density as well as spot size upon
220 stimulation with $G\alpha_i$ or $G\alpha_q$-coupled agonists. However, analysis of the super-resolution 2D STED
221 images shows only an increase in PLCβ3 density without an effect of PLCβ3 spot diameter. These
222 observations suggest that the larger spots observed in the TIRF images are a result of multiple
223 distinct PLCβ3 enzymes within the diffraction limited (~0.250 μm for green dyes) resolution of this
224 approach. Accordingly, in the TIRF analysis, the effects of membrane recruitment are spread
225 across two different measurements, PLCβ3 density and PLCβ3 spot size, whereas in the 2D STED
226 analysis they are consolidated into only effects on PLCβ3 density. This makes the 2D STED
227 analysis more appropriate and robust to assess differences in membrane recruitment. In the 2D
228 STED analysis, stimulation of the $G\alpha_i$-coupled receptor, C5aR, significantly increased the PLCβ3
229 membrane density at 10s, whereas stimulation of the $G\alpha_q$-coupled receptor P2Y6 did not,
230 suggesting that $G\alpha_i$-coupled signaling may be more efficient at recruiting PLCβ3 to the membrane
231 on the functionally relevant timescale in this context.

232 Our experiments demonstrate that $G\alpha_q$ is not required for Gβγ-dependent activation of PLCβ, which
233 is in agreement with other reports using cellular models (12, 13, 30). These observations are also
234 supported by a significant body of work using *in vitro* experiments, which clearly demonstrate that

235 Gβγ alone can robustly activate PLCβ enzymes (1, 2, 8-11). However, these results directly
236 contradict conclusions from previous studies in other model systems showing that $G\alpha_q$ is strictly
237 required (14, 15, 17, 18). The biggest difference in these studies is the cell type and model systems
238 used. We propose that the ability of Gβγ to independently activate PLCβ depends on the free Gβγ
239 concentration resulting from receptor activation, which varies between cell types and activation
240 stimuli (**Fig. 6**). Consistent with this proposal, a growing body of evidence suggests that the ability
241 of $G\alpha_i$-coupled receptors to regulate PLCβ is context dependent and is dictated by the local
242 concentration of Gβγ generated by receptor stimulation (13, 19, 20) (**Fig. 6**). Similar observations
243 were made regarding $G\alpha_i$-coupled stimulation of GIRK channels (31, 32). The effective Gβγ
244 concentration is dependent on several factors, including receptor density and organization, the
245 kinetics of G protein release upon stimulation, and the Gβγ subtype and cellular distribution (19,
246 31, 32). Another factor likely contributing to this capability is the concentration of PLCβ on the
247 plasma membrane at rest, which is proposed to be dictated by subtype and recruitment by
248 additional proteins (3, 5). If sufficient PLCβ is not present on the plasma membrane, the
249 concentration of Gβγ required to shift the equilibrium to membrane-associated PLCβ is higher (**Fig.
250 6**).

251 Such a concentration dependence is less relevant for $G\alpha_q$-dependent stimulation because the
252 affinity of PLCβ for $G\alpha_q$ is much higher than for Gβγ, given that the PLCβ-$G\alpha_q$ complex is stable in
253 the absence of the membrane surface, which supports much higher local concentrations (1, 5).
254 Additionally, our results, in agreement with other recent work (18), show that $G\alpha_q$ signaling also
255 recruits PLCβ to the plasma membrane, providing a mechanism for $G\alpha_q$ to contribute to Gβγ-
256 dependent activation, despite the observations that Gβγ-dependent activation can be independent
257 of $G\alpha_q$. In the case of stimulation with both $G\alpha_q$- and $G\alpha_i$-coupled agonists, $G\alpha_q$ both allosterically
258 activates and recruits PLCβ to the membrane. Thus, dual stimulation would reduce the
259 concentration of Gβγ necessary to form PLCβ-Gβγ complexes where Gβγ can orient the PLCβ
260 catalytic core for catalysis and further shift the PLCβ equilibrium from cytosolic to membrane-
261 associated (**Fig. 6C**). A requirement for dual stimulation would make sense in physiological
262 contexts where PLCβ stimulation would be detrimental to $G\alpha_i$-coupled signaling, for example in
263 GIRK signaling in cardiomyocytes (31, 33). Acetylcholine-induced activation of GIRK channels
264 functions to induce hyperpolarization, which lengthens the interval between cardiac action
265 potentials, thereby reducing heart rate (31, 33). This process is mediated by free Gβγ generated by
266 $G\alpha_i$-coupled acetylcholine receptors, but GIRK channels also require PIP2 to open (34, 35).
267 Therefore, Gβγ-induced PLCβ activation would deplete PIP2 and counteract channel activation.
268 This example highlights the necessity for intricate fine-tuning of PLCβ function, which requires
269 additional layers, including rates of Gβγ release by receptors, the presence of competing Gβγ-
270 binding proteins, and membrane localization of GPCRs and target proteins, to supplement the G
271 protein-dependent regulation. While additional studies are needed to validate this proposal, it is an
272 attractive hypothesis to explain inconsistencies in the literature regarding this system over the last
273 two decades.

274 **Materials and Methods**

275 *Cell Culture*
276 Raw 264.7 cells were obtained from ATCC (TIB-71) and were cultured according to ATCC
277 recommendations. Briefly, they were maintained in Dulbecco's Modified Eagle Medium (GIBCO)
278 supplemented with 10% fetal bovine serum and 2 mM L-glutamine. For passaging, they were
279 detached using a cell scraper. They were tested for mycoplasma during the course of the
280 experiments.

281 *Compound stock concentrations*

282 UDP (disodium salt, Tocris Bioscience 311150) was dissolved in H_2O to make a 20 mM stock,
283 which was diluted into DPBS +Ca^{2+}/Mg^{2+} (Corning) for use in experiments. LPA (18:1 Lyso PA;
284 Avanti Research 857130P-25mg) was dissolved in chloroform and the chloroform was evaporated
285 using a continuous stream of Argon gas to produce a lipid film. The film was washed with pentane,
286 followed by evaporation with Argon gas. The lipid film was rehydrated with H_2O to make a 5 mM
287 stock and sonicated to clarity with a bath sonicator. This stock was further diluted into DPBS
288 +Ca^{2+}/Mg^{2+} (Corning) for use in experiments. C5a was either purchased from abcam (Recombinant
289 human C5a protein ab167724) or purified as described below. Commercial C5a was reconstituted
290 with H_2O at 36 μM and diluted into DPBS +Ca^{2+}/Mg^{2+} (Corning) for use in experiments. U73122
291 (Tocris Bioscience 1268) and negative control U73343 (Tocris Bioscience 4133) was dissolved in
292 chloroform, and the chloroform was evaporated with a continuous stream of Argon gas to produce
293 a film, which was stored at -20°C until use. For experiments, the film was reconstituted in DMSO
294 at 12 mM using a bath sonicator. FR900359 (FR) (caymen chemicals 33666) was dissolved in
295 DMSO to make a stock of 10 mM. YM254890 (YM) (tocris YM254890) was dissolved in DMSO to
296 make a 2 mM stock.

297 *C5a expression and purification*

298 C5a was prepared as described (36). Constructs were synthesized with N-terminal Thioredoxin
299 (Trx) and His tags followed by a 3C precession protease cleavage site and cloned into a Pet28
300 expression vector. SHuffle T7 Express Competent E. coli (NEB) were transformed according to the
301 manufacturer's protocol and incubated at 30°C overnight. Large cultures were grown to an OD_{600}
302 of ~1.0 and induced with 500 mM Isopropyl β-D-1-thiogalactopyranoside (IPTG) at 16°C overnight.
303 Cells were harvested by centrifugation at 3,500 x g for 15 minutes and pellets were flash frozen
304 and stored at -80°C until use. Purification was carried out at 4°C. Cells were resuspended in
305 purification buffer (50 HEPES pH 7.5, 300 mM NaCl) supplemented with 30 mM imidazole, DNase
306 and protease inhibitors (12.5 µg/mL leupeptin, 12.5 µg/mL pepstatin A, 625 µg/mL AEBSF, 1 mM
307 Benzamadine, 100 µg/mL Trypisin inhibitor, 1x aprotinin, and 1 mM PMSF), lysed by sonication,
308 and clarified by centrifugation at 39,000 x g for 45 minutes. Clarified lysate was bound in batch to
309 10 mL NiNTA resin (Qiagen) equilibrated with purification buffer supplemented with 30 mM
310 imidazole for 1 hour. The resin was washed in batch with 100 mL of purification buffer
311 supplemented with 30 mM imidazole then loaded onto a column and washed by gravity flow with
312 10 column volumes of high salt buffer (50 HEPES pH 7.5, 1 M NaCl, 30 mM imidazole) and eluted
313 with purification buffer supplemented with 500 mM imidazole. Eluted protein was concentrated to
314 ~2 mL using a 15-mL Amicon concentrator with 10-kDa molecular weight cutoff, then diluted to ~25
315 mL using purification buffer without imidazole and incubated with 3C precession protease (prepared
316 in-house) overnight at 4°C remove the Txr and His tags. The cleaved protein was passed over a
317 column of 10 mL NiNTA resin equilibrated with purification buffer supplemented with 35 mM
318 imidazole three times to remove the free Trx-His and concentrated to 1 mL using a 15-mL Amicon
319 concentrator with 3-kDa molecular weight cutoff. C5a was purified further via size exclusion
320 chromatography using a Superdex 75 10/300 increase column equilibrated with purification buffer.
321 Fractions containing C5a were pooled and concentrated to ~0.8 mg/mL using a 4-mL Amicon
322 concentrator with 3-kDa molecular weight cutoff and flash frozen and stored at -80°C until use.

323 *Ca^{2+} mobilization*

324 For Ca^{2+}mobilization experiments, Raw 264.7 cells were seeded in black, clear bottom, poly-L-
325 lysine coated 384 well plates (20 μL of cells at $0.7*10^6$ cells/mL) for at least 12-18 hours prior to
326 the experiment. Cells were loaded with 20 μL of 2X Fluo-4 supplemented with 5 mM water soluble
327 probenecid using the Fluo-4 Direct™ Calcium Assay Kit (Invitrogen) for 2 hours at room
328 temperature protected from light. Fluorescence was monitored with excitation at 470 nm emission
329 at 540 nm using a Hammamatsu μCell FDSS system with a sampling interval of 0.32 s. Agonists
330 were automatically injected and mixed with continuous reading during the measurements. Final

concentrations added were as follows: 10 μM UDP, 20 nM C5a, 5 μM LPA or 20 nM C5a+10 μM UDP.

For experiments with U73122 (20 μM), U73343 (20 μM), FR (10 μM), YM (500 nM), and DMSO (0.5%), compounds were diluted into the 2X Fluo-4 loading solution and incubated during the loading (2 hours at room temperature). DMSO was kept at or below 0.5% final concentration, which did not influence signaling responses (**Fig. S1**). PTX (Sigma, P2980-50UG) was added into the culture medium at 200 ng/mL for overnight incubation and added into the 2X Fluo-4 loading solution during the loading (2 hours at room temperature), for a final concentration of 300 ng/mL

Raw fluorescence traces were baseline subtracted and averaged over 8-12 wells for each experiment. For comparison, the peak heights from each individual trace were averaged to determine a final value for the peak height for each condition. The linear component of the peak increase was fit for each set of averaged traces with each technical repeat treated separately. Conditions were repeated at least 3 times with 2 technical replicates per biological replicate resulting in a total of $n \geq 6$ averaged repeats.

Immunolabeling

For immunolabeling, precision cover glass #1.5H (Thorlabs) coverslips were sterilized with ethanol, placed in the wells of a 24-well plate, and coated with poly-L-Lysine. Cells were seeded into wells with coverslips (0.5 mL of cells at $0.2*10^6$ cells/mL to ensure well-separated single cells for imaging) for 12-18 hours prior to the experiment.

All washes/incubations were 0.5 mL with gentle rocking unless otherwise noted. For immunolabeling, culture media was removed and cells were washed with DPBS containing Ca^{2+}/Mg^{2+} (Corning, used throughout this procedure) for 5 minutes. Agonists for stimulation were diluted in DPBS at the following concentrations: 10 μM UDP, 20 nM C5a, or 20 nM C5a+10 μM UDP. Agonists were added and incubated for the desired stimulation time and fixing was initiated with 8% PFA for 5 minutes with gentle rocking. The solution was exchanged for DPBS+4% PFA and incubated for 10 minutes. Cells were washed twice with DPBS for 5 minutes and permeabilized with DPBS supplemented with 2% BSA (DPBS+BSA) and 0.5% Triton X-100 for 10 minutes. The Triton X-100 was washed out with DPBS+BSA and incubated for 20 minutes. Cells were washed an additional time with DPBS+BSA and incubated with primary antibodies (see **Table 1**) for 1 hour. The cells were washed 3 times with DPBS+BSA for 5 minutes each and incubated with secondary antibodies (see antibodies table) for 1 hour protected from light. The cells were washed 3 times with DPBS+BSA for 5 minutes each and re-fixed with DPBS+BSA supplemented with 4% PFA for 10 minutes. The PFA was washed out twice with DPBS+BSA and coverslips were mounted on glass slides with ProLong diamond antifade mountant (Invitrogen) and sealed immediately with nail polish to prevent curing, 3D flattening and to retain a lower refractive index required for TIRF microscopy. Slides were stored to 4°C and imaged within a week of preparation. Stimulation time courses were completed with two biological repeats with two technical repeats for each biological repeat.

TIRF imaging

TIRF imaging was performed using an inverted widefield fluorescence microscope stand (Nikon ECLIPSE Ti2) equipped with motorized XY stage, Perfect Focus System (PFS), and a iLas 2 (Gataca Systems) illumination device allowing Azimuthal TIRF imaging (ring-TIRF), a specialized TIRF microscopy technique designed to improve illumination uniformity of evanescent wavefront by reduction of interference artifacts. This system allows highly calibrated imaging depth control from widefield epifluorescence, to Highly Laminated Optical Sheet imaging (HILO, an oblique illumination technique), to TIRF imaging down to ~70 nm shallow depth of field. The system is equipped with 488/561/640 nm diode lasers and appropriate excitation and emission filters for 3-color TIRF imaging. 1200X1200 pixel frames of images were acquired through a CFI Apochromat

379 TIRF 100XC NA 1.49 Oil objective lens (Nikon) with motorized correction collar on a Orca Fusion
380 sCMOS camera (Hamamatsu) with 6.5 µm pixel pitch, using NIS Elements v5.42.06 (Nikon)
381 software suite. Images were saved as the system default ".nd2" file format that retains all image
382 metadata.

383 *STED imaging*

384 STED imaging was performed on an inverted IX81 microscope stand (Olympus, now Evident
385 Scientific), equipped with motorized X,Y stage, Zero Drift Compensation hardware based autofocus
386 (ZDC2), and a Facility Line STED system (Abberior) with a pulsed 775nm depletion laser and
387 405nm, as well as pulsed 488/561/640 nm excitation laser lines. Spatial Light Modulators (SLM)
388 generated specific 2D/3D STED depletion beam patterns that were delivered to the stand via a
389 single beam path with a deformable mirror adaptive optical accessory to correct for refractive index
390 mismatch and spherical aberrations. Images were acquired using Imspector LightBox software v.
391 16.3.14287-w2129 (Abberior), and an UPLXAPO100X 1.45 NA oil immersion objective (Olympus,
392 now Evident Scientific) and 3D STED was performed using a mix of 90% 3D and 10% 2D depletion
393 patterns, while keeping the pinhole closed to ~0.7 AU. Images were acquired on separate spectrally
394 gated Avalanche Photodiode detectors (APDs) using 650-755 nm band pass for STAR RED and
395 588-698 nm band pass for Alexa Fluor® 594. Image pixel/step sizes were calculated to satisfy the
396 Nyquist sampling criteria using an online calculator tool (https://svi.nl/Nyquist-Calculator), and all
397 images were collected using the same settings for excitation and depletion laser powers, pinhole
398 diameter, line accumulation and pixel dwell times. Acquired images were saved as the default ".obf"
399 files that retain all image metadata.

400 *Image processing and analysis*

401 Images were processed and analyzed using Huygens Professional v25,10 (SVI). Templates were
402 generated for microscopy parameters based on image metadata, and for deconvolution using an
403 appropriate point spread function (PSF) model for automatically computing a theoretical PSF from
404 microscopic parameters and a model of the microscope. All images were batch processed for
405 consistency using the templates in Huygens Workflow processor. The deconvolved images were
406 further corrected for chromatic aberrations and analyzed using Huygens Object Analyzer advanced
407 module. Appropriate thresholds and seeds for intensity masks were determined empirically at first,
408 with automatic Otsu's thresholding as a starting point, and the segmentation quality were fine-tuned
409 further using Gaussian filtering with a low sigma radius and watershed fragmentation with sparse
410 seeding. All comparable images were segmented with identical parameters and measurements
411 were extracted for the reported parameters as ".csv" files for further analysis.

412 For TIRF images, full image frames were cropped to individual cells and subjected to express
413 deconvolution using Huygens Professional before processing and analysis as described above.
414 Within the object analyzer, cell boundaries were manually traced using the C5aR signal and the
415 PLCβ spots/area and spot diameter were measured. At least three images for each technical repeat
416 were collected, resulting in n=12 images/time point. At least two cells were cropped from each
417 image, resulting in n>24 cells/time point in the final statistics shown in **Fig. 3**.

418 For 3D STED axial line scans, the plasma membrane was manually traced using the C5aR signal
419 and the percentage of PLCβ puncta within 100nm of this tracing was measured. At least 4 images
420 for each technical repeat were collected, resulting in n>16 for each condition in the final statistics
421 in **Fig. 4**.

422 For 2D STED analysis, images were cropped in z to include only the plasma membrane proximal
423 part of the Z-stack using the C5aR signal as a guide. Density of C5aR and PLCβ spots was
424 determined within the cropped image volume, and the X-Y diameter of each spot was reported. To
425 ensure the results were not dependent on the thresholding used, results for two different
426 segmentation parameters are reported (**Fig. S4**). At least three images for each technical repeat

were collected, resulting in n ≥ 6 images for each condition in the final statistics in **Fig. 5** and **S4-S5**.

Two-sample Student's t-test were completed with a null hypothesis that the difference between the means is 0 to assess the statistical significance of each time point from the nonstimulated condition. P values are indicated directly on the graphs.

Acknowledgments

All microscopy work was performed in the Bio-Imaging Resource Center at Rockefeller University, RRID:SCR_017791. We thank Alison North and other members for their assistance with fluorescence imaging experiments and data analysis. We thank Chloe Larson and other members from the Fisher Drug Discovery Resource Center of the Rockefeller University for help and resources to complete the Ca^{2+} mobilization experiments. We thank members of the MacKinnon lab, Jue Chen, and members of her research group for helpful discussions. This work was supported by National Institute of General Medical Sciences (NIHF32GM142137 to MEF). RM is an investigator in the Howard Hughes Medical Institute. Some figures were created using BioRender.com.

Data, Materials, and Software Availability

All data is available from the authors upon request.

References

1. M. E. Falzone, R. MacKinnon, The mechanism of Gα _q regulation of PLCβ3 -catalyzed PIP2 hydrolysis. *Proceedings of the National Academy of Sciences* **120**, e2315011120 (2023).
2. Maria E. Falzone, R. MacKinnon, Gβγ activates PIP2 hydrolysis by recruiting and orienting PLCβ on the membrane surface. *Proceedings of the National Academy of Sciences* **120**, e2301121120 (2023).
3. A. M. Lyon, J. J. G. Tesmer, Structural insights into phospholipase C-β function. *Molecular Pharmacology* **84**, 488-500 (2013).
4. G. Kadamur, E. M. Ross, Mammalian Phospholipase C. *Annual Review of Physiology* **75**, 127-154 (2013).
5. S. Ubeysinghe, D. Wijayaratna, D. Kankanamge, A. Karunarathne, "Chapter Two - Molecular regulation of PLCβ signaling" in Methods in Enzymology, A. K. Shukla, Ed. (Academic Press, 2023), vol. 682, pp. 17-52.
6. P. Kemp, G. Hübscher, J. Hawthorne, Phosphoinositides. 3. Enzymic hydrolysis of inositol-containing phospholipids. *Biochemical Journal* **79**, 193-200 (1961).
7. R. Rodnight, Cerebral diphosphoinositide breakdown: activation, complexity and distribution in animal (mainly nervous) tissues. *Biochemical Journal* **63**, 223-231 (1956).
8. M. Camps *et al.*, Isozyme-selective stimulation of phospholipase C-β2 by G protein βγ-subunits. *Nature* **360**, 684-686 (1992).
9. A. Katz, D. Wu, M. I. Simon, Subunits βγ of heterotrimeric G protein activate β2 isoform of phospholipase C. *Nature* **360**, 686-689 (1992).
10. A. V. Smrcka, P. C. Sternweis, Regulation of purified subtypes of phosphatidylinositol-specific phospholipase C β by G protein α and βγ subunits. *Journal of Biological Chemistry* **268**, 9667-9674 (1993).
11. S. N. Hicks *et al.*, General and Versatile Autoinhibition of PLC Isozymes. *Molecular Cell* **31**, 383-394 (2008).
12. T. I. A. Roach *et al.*, Signaling and cross-talk by C5a and UDP in macrophages selectively use PLCβ3 to regulate intracellular free calcium. *Journal of Biological Chemistry* **283**, 17351-17361 (2008).

13. Z.-G. Gao, R. R. Gao, C. K. Meyer, K. A. Jacobson, A2B adenosine receptor-triggered intracellular calcium mobilization: Cell type-dependent involvement of Gi, Gq, Gs proteins and protein kinase C. *Purinergic Signalling* 10.1007/s11302-025-10070-1 (2025).
14. E. M. Pfeil *et al.*, Heterotrimeric G Protein Subunit Gαq Is a Master Switch for Gβγ-Mediated Calcium Mobilization by Gi-Coupled GPCRs. *Molecular Cell* 10.1016/j.molcel.2020.10.027, 1-15 (2020).
15. G. Sanchez, E. M. Jutkiewicz, S. L. Ingram, A. V. Smrcka, Coincident Regulation of PLCβ Signaling by Gq-Coupled and μOpioid Receptors Opposes Opioid- Mediated Antinociception. *Molecular Pharmacology* 10.1124/molpharm.122.000541 (2022).
16. T. Takano *et al.*, Pancreatic acinar cell signalling and function exhibit an absolute requirement for activation of Gα_q. *The Journal of Physiology* **603**, 4497-4514 (2025).
17. J. Brands *et al.*, A molecular mechanism to diversify Ca2+ signaling downstream of Gs protein-coupled receptors. *Nature Communications* **15**, 7684 (2024).
18. K. Senarath *et al.*, An integrated mechanism of Gq regulation of PLCβ enzymes. *Proceedings of the National Academy of Sciences* **122**, e2500318122 (2025).
19. K. Senarath *et al.*, Gγ identity dictates efficacy of Gβγ signaling and macrophage migration. *Journal of Biological Chemistry* **293**, 2974-2989 (2018).
20. P. Siripurapu, D. Kankanamge, K. Ratnayake, K. Senarath, A. Karunarathne, Two independent but synchronized Gβγ subunit-controlled pathways are essential for trailing-edge retraction during macrophage migration. *Journal of Biological Chemistry* **292**, 17482-17495 (2017).
21. L. Zhu, C. Jones, G. Zhang, The Role of Phospholipase C Signaling in Macrophage-Mediated Inflammatory Response. *Journal of Immunology Research* **2018**, 5201759 (2018).
22. M. Cedzyński, N. M. Thielens, T. E. Mollnes, T. Vorup-Jensen, Editorial: The Role of Complement in Health and Disease. *Frontiers in Immunology* **10**, 1869 (2019).
23. D. Klaver, M. Thurnher, Control of Macrophage Inflammation by P2Y Purinergic Receptors. *Cells* **10**, 1098 (2021).
24. S. Jiang, H. Yang, M. Li, Emerging Roles of Lysophosphatidic Acid in Macrophages and Inflammatory Diseases. *International Journal of Molecular Sciences* **24**, 12524 (2023).
25. M. Tennakoon, D. Kankanamge, K. Senarath, Z. Fasih, A. Karunarathne, Statins Perturb G βγ Signaling and Cell Behavior in a G γ Subtype Dependent Manner. *Molecular Pharmacology* **95**, 361-375 (2019).
26. R. Schrage *et al.*, The experimental power of FR900359 to study Gq-regulated biological processes. *Nature Communications* **6**, 10156 (2015).
27. S. Mangmool, H. Kurose, Gi/o Protein-Dependent and -Independent Actions of Pertussis Toxin (PTX). *Toxins* **3**, 884-899 (2011).
28. M. Oheim, A. Salomon, A. Weissman, M. Brunstein, U. Becherer, Calibrating Evanescent-Wave Penetration Depths for Biological TIRF Microscopy. *Biophysical Journal* **117**, 795-809 (2019).
29. A. Barbotin *et al.*, z-STED Imaging and Spectroscopy to Investigate Nanoscale Membrane Structure and Dynamics. *Biophysical Journal* **118**, 2448-2457 (2020).
30. Z.-G. Gao, K. A. Jacobson, On the selectivity of the Gαq inhibitor UBO-QIC: A comparison with the Gαi inhibitor pertussis toxin. *Biochemical Pharmacology* **107**, 59-66 (2016).
31. K. K. Touhara, R. MacKinnon, Molecular basis of signaling specificity between GIRK channels and GPCRs. *eLife* **7**, 1-23 (2018).
32. Y. Zhang, R. MacKinnon, Higher-order transient structures and the principle of dynamic connectivity in membrane signaling. *Proceedings of the National Academy of Sciences* **122**, e2421280121 (2025).
33. N. Schmitt, M. Grunnet, S.-P. Olesen, Cardiac Potassium Channel Subtypes: New Roles in Repolarization and Arrhythmia. *Physiological Reviews* **94**, 609-653 (2014).
34. W. Wang, K. K. Touhara, K. Weir, B. P. Bean, R. MacKinnon, Cooperative regulation by G proteins and Na+ of neuronal GIRK2 K+ channels. *eLife* **5**, 1-15 (2016).

528 35. W. Wang, M. R. Whorton, R. MacKinnon, Quantitative analysis of mammalian GIRK2
529 channel regulation by G proteins, the signaling lipid PIP2 and Na+ in a reconstituted
530 system. *eLife* **3**, e03671 (2014).
531 36. Y. Feng *et al.*, Mechanism of activation and biased signaling in complement receptor
532 C5aR1. *Cell Res* **33**, 312-324 (2023).

533

Figures and Tables

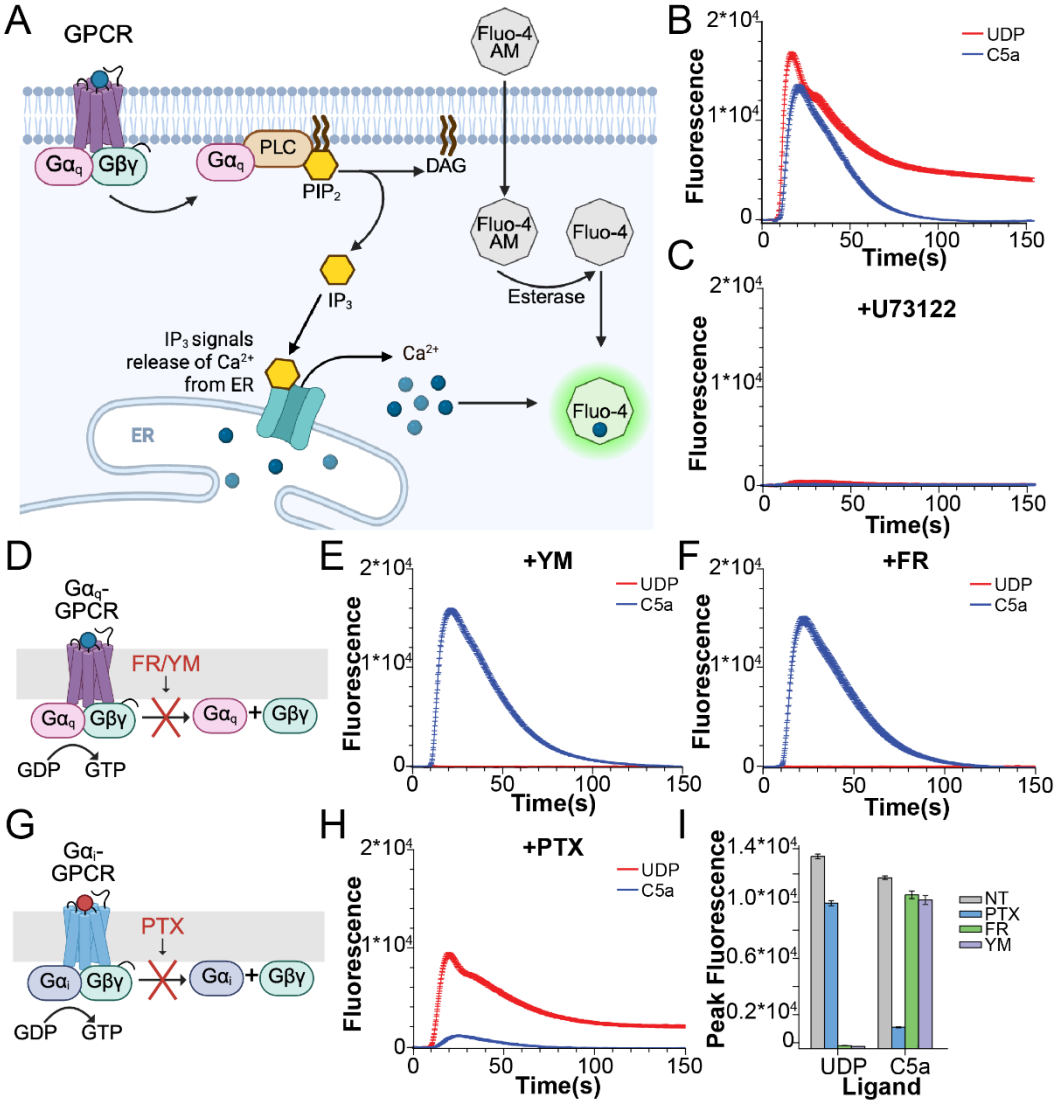

Figure 1: PLCβ-dependent signaling in Raw264.7 cells. **A**: Cartoon of fluo-4 Ca^{2+} assay for PLCβ activity. Fluo-4 AM is loaded into cells and esterases cleave the hydrophobic groups, trapping it inside. GPCR stimulation activates PLCβ, which generates IP3, resulting in Ca^{2+} release from the ER through the IP3 receptor and increases the fluorescence signal. **B-C**: Representative Ca^{2+} transients upon stimulation with UDP (red) and C5a (blue) in the absence (B) or presence (C) of PLCβ inhibitor U73122 (20 μM). **D**: Cartoon representation of the effects of $G\alpha_q$ cyclic peptide inhibitors FR/YM. **E-F**: Representative Ca^{2+} transients upon stimulation with UDP (red) and C5a (blue) in the presence of $G\alpha_q$ inhibitors FR (10 μM) (E) or YM (500 nM) (F). **G**: Cartoon representation of the effects of $G\alpha_i$ signaling inhibitor PTX. **H**: Representative Ca^{2+} transients upon stimulation with UDP (red) and C5a (blue) in the presence of 300 ng/mL PTX. **I**: Quantification of Ca^{2+} peak fluorescence for UDP and C5a in the presence of PTX, FR, or YM. Error bars are SEM. For B-C, E-F, and H, traces are averaged from 10 wells and error bars are SEM. UDP was added at 10 μM and C5a at 20 nM final concentrations.

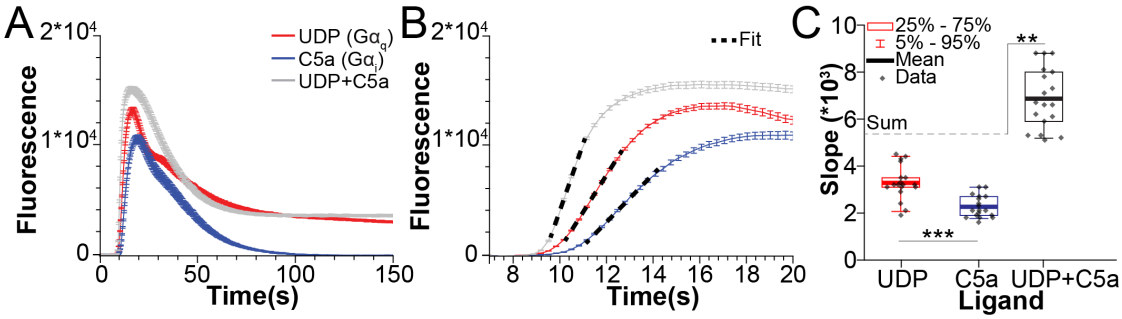

Figure 2: Effects of dual stimulation of $G\alpha_i$ and $G\alpha_q$-coupled receptors on PLCβ activity. **A-B**: Representative Ca^{2+} transients upon stimulation with UDP (red), C5a (blue), or UDP+C5a (gray) for the complete time course (A) or for early times (B). Traces are averaged from 10 wells and error bars are SEM. UDP was added at 10 μM and C5a at 20 nM final concentrations. Fits of the increase to a straight line are shown as a black dashed line in B. **C**: Slopes from the fits in B. The average of the sums of UDP and C5a alone is denoted with a gray dashed line. *: 0.05>p>0.005. **: 0.005>p>0.0005, ***: p<0.0005.

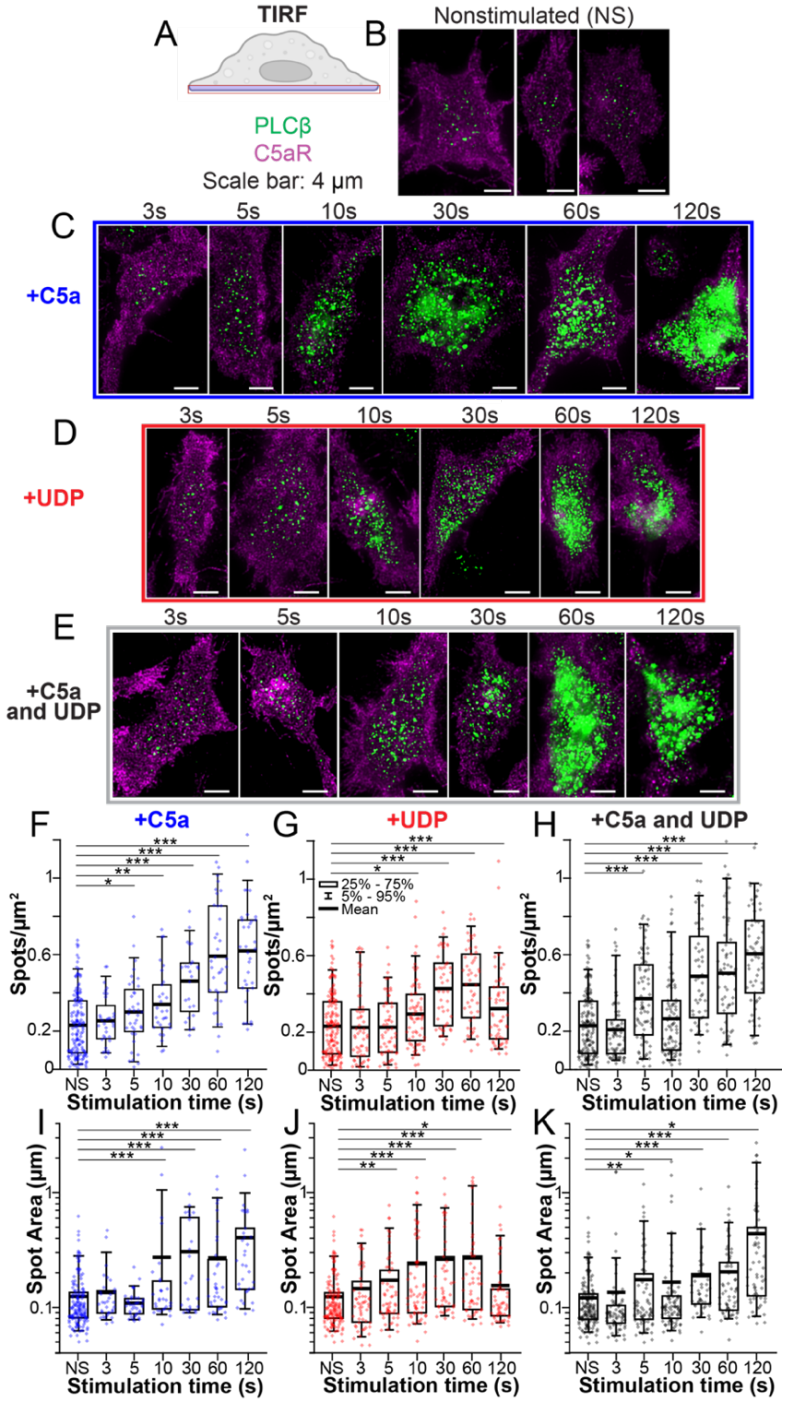

Figure 3: GPCR signaling recruits PLCβ3 to the plasma membrane. **A**: Cartoon of the TIRF imaging plane. **B-E**: Representative images of cells stained for PLCβ3 (green) or C5aR (purple) as a membrane marker in the absence of stimulation (B) or following stimulation with 20 nM C5a (C), 10 μM UDP (D), or UDP+C5a (E). Scale bar is 4 μm. Time points indicate the time of agonist exposure prior to cell fixation. **F-H**: Quantification of PLCβ3 spot density over time upon stimulation with C5a (F), UDP (G), or UDP+C5a (H). **I-K**: Quantification of PLCβ3 spot size over time upon stimulation with C5a (I), UDP (J), or UDP+C5a (K). NS is nonstimulated. Each point is a single cell. *: 0.05>p>0.005. **: 0.005>p>0.0005, ***: p<0.0005.

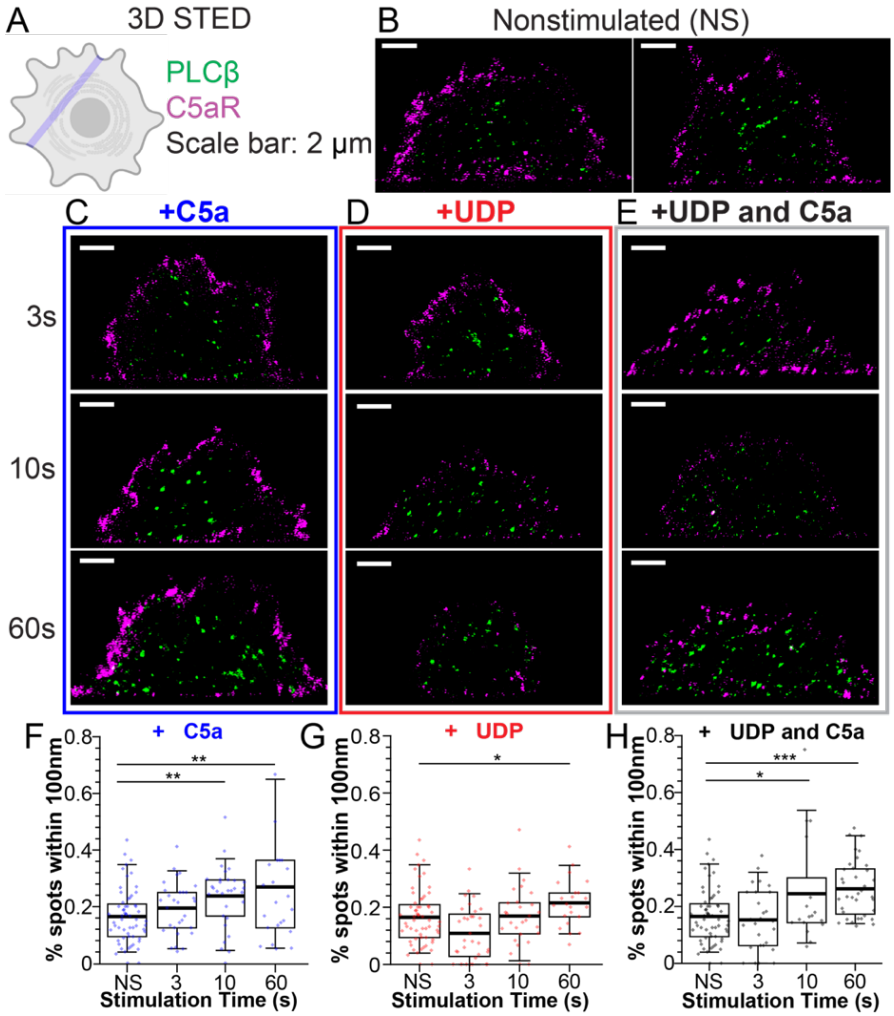

Figure 4: The majority of PLCβ3 is localized in the interior of the cell at rest. **A**: Cartoon of 3D STED linescan imaging plane. **B-E**: Representative images of cells stained for PLCβ3 (green) or C5aR (purple) as a membrane marker in the absence of stimulation (B) or following stimulation with 20 nM C5a (C), 10 μM UDP (D), or UDP+C5a (E). Scale bar is 2 μm. Time points indicate the time of agonist exposure prior to cell fixation. **F-H**: Quantification of percentage of PLCβ3 spots within 100 nm of the plasma membrane over time upon stimulation with C5a (F), UDP (G), or UDP+C5a (H). NS is nonstimulated. Boxes are 25%-75%, error bars are 5%-95%, thick bar is the mean. Each point is a single linescan. *: 0.05>p>0.005. **: 0.005>p>0.0005, ***: p<0.0005.

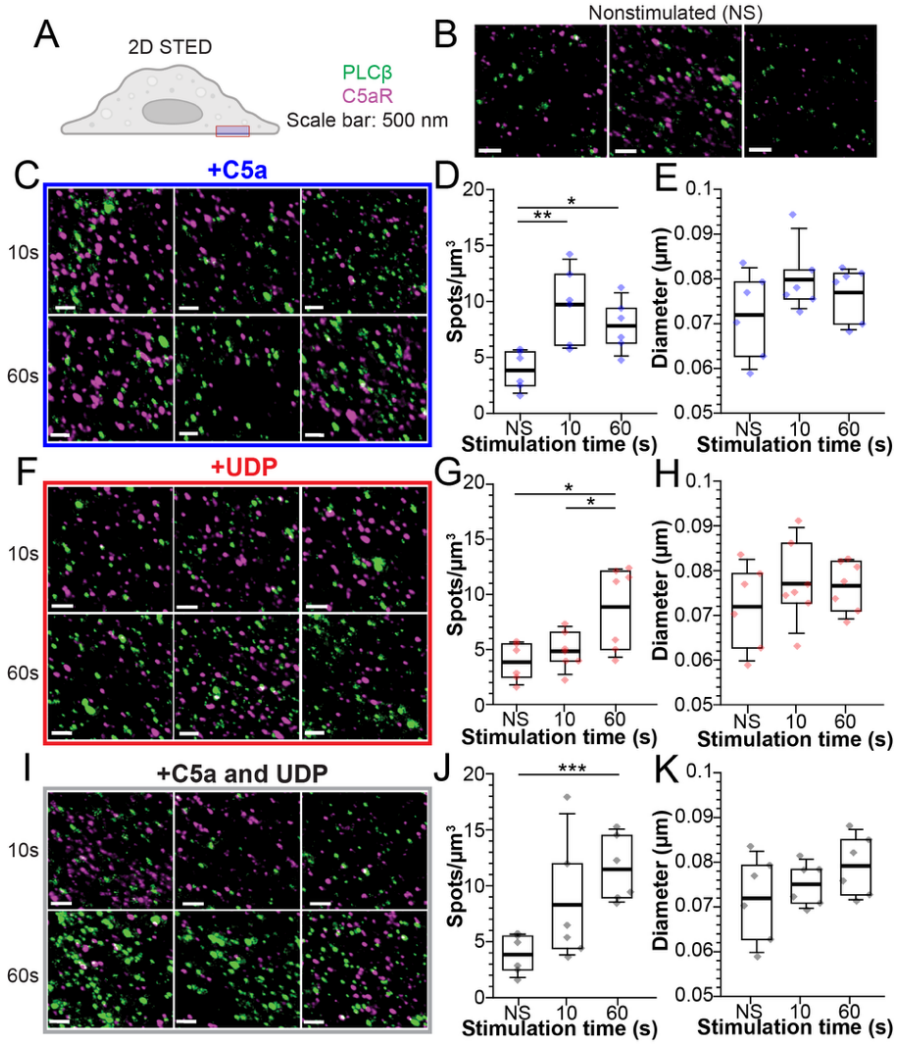

Figure 5: 2D STED demonstration of GPCR-dependent PLCβ3 membrane recruitment. **A**: Cartoon of the 2D STED imaging plane. **B,C,F,I**: Representative images of cells stained for PLCβ3 (green) or C5aR (purple) as a membrane marker in the absence of stimulation (B) or following stimulation with 20 nM C5a (C), 10 μM UDP (D), or UDP+C5a (E). Scale bar is 500 nm. Time points indicate the time of agonist exposure prior to cell fixation. Images are maximum intensity projections of Z stacks for representative purposes. **D,G,J**: PLCβ spot density on the plasma membrane over time upon stimulation with C5a (D), UDP (G), or UDP+C5a (J). **E,H,K**: Quantification of PLCβ3 X-Y diameter over time upon stimulation with C5a (E), UDP (H), or UDP+C5a (K). NS is nonstimulated. Boxes are 25%-75%, error bars are 5%-95%, thick bar is the mean. Each point is a single z stack. *: 0.05>p>0.005. **: 0.005>p>0.0005, ***: p<0.0005.

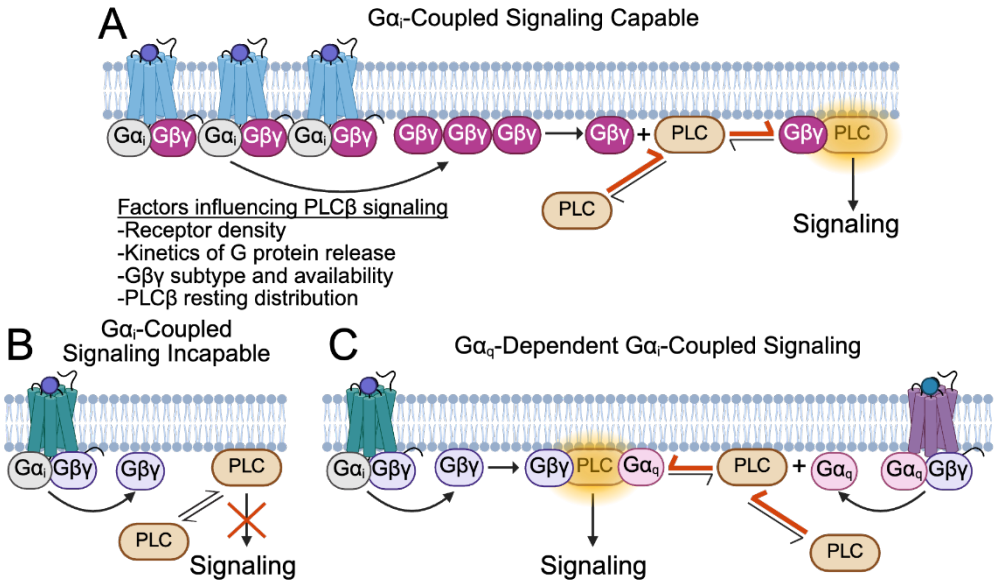

Figure 6: $G\alpha_i$-induced PLCβ signaling is context dependent. **A:** In signaling capable contexts, the receptor density, kinetics of G protein release, Gβγ subtype and availability, and PLCβ resting distribution allow for sufficient Gβγ to be released upon receptor stimulation. This Gβγ recruits PLCβ to the membrane resulting in higher activity and thereby shifting its equilibrium from cytosolic to more membrane associated (red arrows). **B:** In signaling incapable contexts, the generated Gβγ is not sufficient to recruit PLCβ to the membrane so signaling does not occur. **C**: In $G\alpha_q$-dependent contexts, released $G\alpha_q$ recruits additional PLCβ to the membrane (red arrows) and also increases PLCβ catalytic rate (1, 2), rendering the previously insufficient Gβγ concentration able to promote signaling.

597 **Table 1.** Antibodies: Information for antibodies used.

Name	Source	Product number	Concentration
Anti-Phospholipase C beta 3 (rabbit)	Abcam	ab251862	1:200
Anti-C5a-R antibody [10/92] (rat)	Abcam	ab117579	1:500
Goat Anti-Rabbit IgG H&L (Alexa Fluor® 488)	Abcam	ab150077	1:500
Abcam Goat Anti-Rat IgG H&L (Alexa Fluor® 594)	Abcam	ab150160	1:500
abberior STAR RED, goat anti-rabbit IgG	Abberior	STRED-1002-500UG	1:500

598